Supporting Information

Photo-Carrier Multi-Dynamical Imaging at the Nanometer Scale in Organic and Inorganic Solar Cells

Pablo A. Fernández Garrillo[abc], *Łukasz Borowik**[ab], *Florent Caffy*[c], *Renaud Demadrille*[c], *and Benjamin Grévin**[c]

[a] Univ. Grenoble Alpes, F-38000 Grenoble, France.

[b] CEA, LETI, MINATEC Campus, F-38054 Grenoble, France.

[c] CEA, CNRS, Univ. Grenoble Alpes INAC-SPrAM, F-38000 Grenoble, France.

* E-mail: benjamin.grevin@cea.fr

* E-mail: lukasz.borowik@cea.fr

Content

1 Bulk heterojunctions: material synthesis and processing

For the preparation of the polymer PDBS-TQx, we have selected a quinoxaline motif as electron-deficient unit (A) and a dibenzosilole (D) unit as electron-rich one; we also used a thiophene spacer between D and A units. The synthesis of PDBS-TQx was achieved by a Suzuki coupling poly-condensation between the 5,5-dihexyl-3,7-bis(4,4,5,5-tetramethyl-1,3,2-dioxaborolan-2-yl)-5H-dibenzo[b,d]silole and the corresponding dibromoquinoxaline building blocks using Pd2(dba)3/tBu3PHBF4 as catalyst. The synthetic conditions can be found elsewhere.[1] PDBS-TQx belongs to the wide band-gap semiconductors materials family, and it shows an absorption edge in the visible close to 650 nm corresponding to an optical bandgap of 1.97 eV. When PDBS-TQx is combined with $PC_{71}BM$ to fabricate bulk-heterojunction solar cells, PCE up to 5.14% can be achieved.[1]

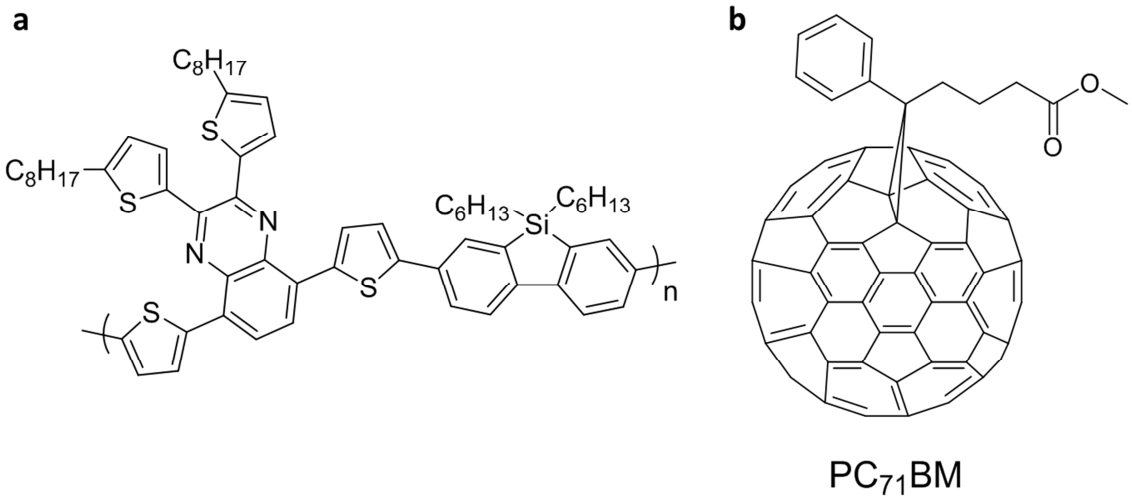

Scheme S1. a) Chemical structures of the electron donor polymer PDBS-TQx. b) electron-acceptor molecule $PC_{71}BM$

2 Surface photo-voltage polarities on organic blends and poly-crystalline silicon

In our work, negative and positive shifts of the KPFM surface potential are observed under illumination on the donor-acceptor organic blends and on the poly-crystalline silicon thin film, respectively. Here, we briefly justify these polarities with respect to the setup geometry, and the nature of the investigated samples. First, we remind that the KPFM compensation bias is applied to the cantilever in our setups, while the ground contact is applied to the substrate. Hence, the KPFM bias yields a direct measurement of the surface potential. In other words, a positive shift of the local vacuum energy level[2] results in a negative shift of the tip compensation bias.

In the case of the organic donor-acceptor blend, the surface photo-voltage originates from the splitting of electrons and holes quasi Fermi levels under illumination.[3] In the following we consider a simplified band alignment model (Figure S1a) with respect to the substrate. In the dark state, the Fermi level of the donor is pinned by the substrate, while the acceptor displays a flat band alignment. Under illumination, the holes quasi-Fermi level remains aligned with the Fermi level of the grounded substrate, while the electrons quasi-Fermi level is located near the lowest unoccupied orbital level (LUMO) of the acceptor. As a consequence, the local vacuum level remains constant over the donor units, and is shifted upward over the acceptor segments. If the morphology of the blend is not "fully inverted[4]", this should result in a global positive shift of the local vacuum level under illumination, compensated by a negative shift of the KPFM regulation bias, *i.e.* a negative surface photo-voltage. We also checked the validity of this argument by measuring KPFM surface photo-voltages on full operating solar cells with a top-metallic electrode (not shown). Negative shifts were observed, and the SPV values were found to be fully consistent with the open circuit voltage values measured by conventional electrical characterization.

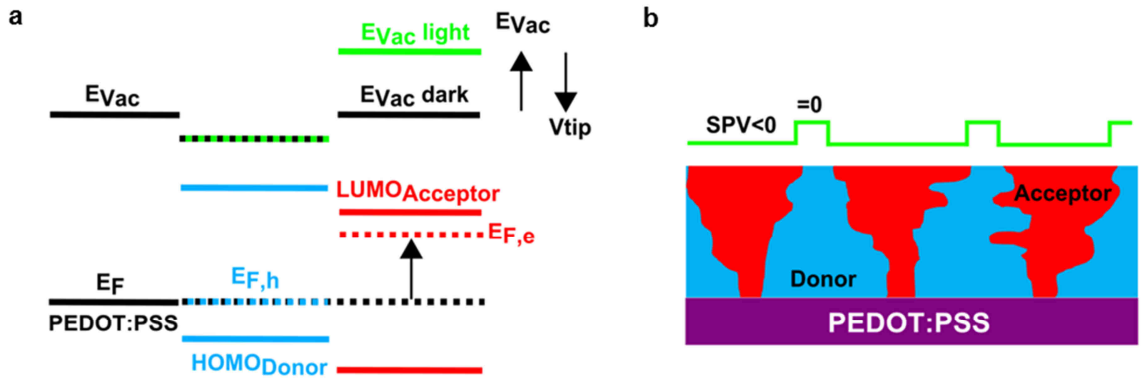

Figure S1. a) Schematic representation of the donor and acceptor molecular levels alignment with respect to the Fermi level of the PEDOT:PSS substrate. HOMO: highest occupied molecular orbital. LUMO: lowest unoccupied molecular orbital. Here, we assume a Fermi level pinning of the electron donor material and a flat band alignment of the acceptor material. Under illumination, the local vacuum level (E_{Vac}) remains constant over the donor while it is shifted upward over the acceptor, resulting in a negative shift of the surface potential in average. E_F: Fermi level. E_F,h (E_F,e): holes (electrons) quasi Fermi level. b) Schematic representation of the donor-acceptor blend morphology. The electron-donor and electron-acceptor materials are represented in blue and red, respectively.

With regards to the polycrystalline silicon sample, the observed positive surface photo-voltage is also fully consistent with the band alignment at the interface between the grounded substrate (n-doped Si) and the non-doped polycrystalline silicon, as shown by Figure S2. Under illumination, the holes generated in the n-doped substrate are injected in the polycrystalline layer due to the internal electric field caused by the band bending at the n-Si/Si interface. This results in a global positive photo-charging of the poly-Si layer.

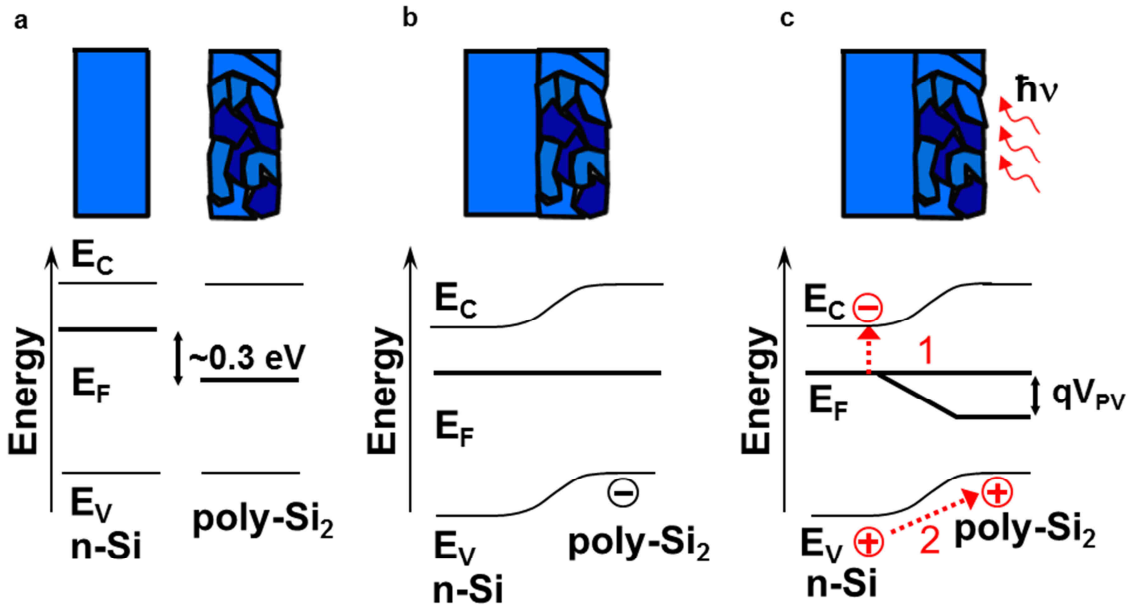

Figure S2. Schematic illustrations of the energy band diagrams for the n-doped silicon substrate (n-Si) and the poly-crystalline silicon thin film (poly-Si). a) Hypothetic case without contact. The 0.3 eV shift between the Fermi levels is due to the doping ($1015cm^{-3}$) of the n-Si substrate. b) Fermi level alignment and band bending under contact (dark state). c) Under illumination, the holes accumulate in the poly-Si due to the internal electric field at the n-Si/poly-Si interface.

3 Fitting the average surface photo-potential as a function of the illumination modulation frequency with simple exponentials

Under modulated illumination the KPFM regulation loop yields an average value V_{av} of the surface potential. In first approximation, we will use simple exponential functions with characteristic time constants τb and τd to describe the surface photo-voltage (SPV) built-up (τb) and decay (τd) dynamics:

$$0 \le t \le D/f \qquad SPV(t) = V(t) - V_D = K_1\left(1 - e^{\frac{-t}{\tau_b}}\right) + K_2 \tag{S1}$$

$$D/f \le t \le 1/f \qquad SPV(t) = V(t) - V_D = K_3 e^{-\frac{t-\frac{D}{f}}{\tau_d}} \tag{S2}$$

With $$K_1 + K_2 = SPV_{\max};\ K_3 = SPV_{\max 1}\left(1 - e^{\frac{-D}{f\ \tau_b}}\right);\ K_2 = K_3 e^{-\frac{1-\frac{D}{f}}{\tau_d}}$$

Here, f and D represent the modulation frequency and duty ratio, respectively. $V(t)$ and $SPV(t) = V(t) - V_D$ are the instantaneous surface potential and surface photo-voltage at a given time t. V_D is the in-dark surface potential, and SPV_{max} is the maximum surface photo-voltage that would be measured under continuous wave illumination. The constants K_1, K_2 and K_3 are fixed such a way that i) if τb approaches zero, the SPV is equal to SPV_{max} when the light is on (case of an "instantaneous" photo-charging) ii) the instantaneous photo-potential present no discontinuity at $t = D/f$

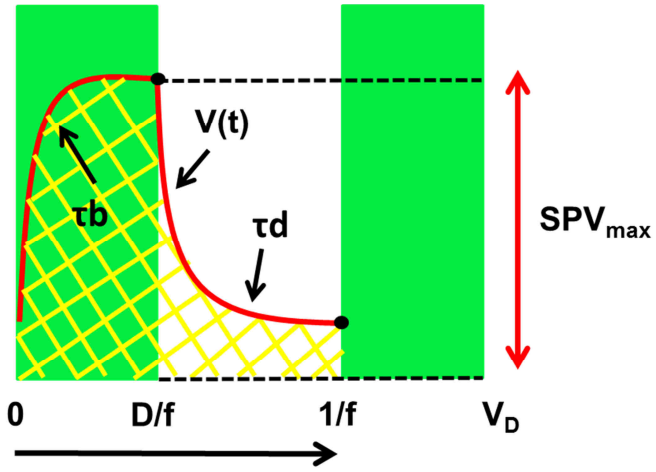

Figure S3. The average potential probed by KPFM V_{av} is obtained by integrating the instantaneous surface potential V(t) (red line) over one modulation cycle. Note that the surface photo-voltage is referenced with respect to the in-dark potential V_D.

The average surface potential V_{av} is calculated (Figure S3) by integrating SPV(t) over one period of the modulation signal $T = 1/f$:

$$V_{av} = f\left[\frac{V_D}{f} + \int_0^{D/f}[V(t)]dt + \int_{D/f}^{1/f}[V(t)]dt\right] \quad \text{(S3)}$$

Solving the integrals yields:

$$V_{av} = V_D + SPV_{\max} D\left(1 - e^{\frac{-D}{f\tau_b}} e^{\frac{-(1-D)}{f\tau_d}}\right) + SPV_{\max}\left(f\tau_d - f\tau_b\right)\left(1 - e^{\frac{-D}{f\tau_b}}\right)\left(1 - e^{\frac{-(1-D)}{f\tau_d}}\right) \quad \text{(S4)}$$

4 Case of an "instantaneous" photo-charging

In the limit where τb approaches zero, the latter equation becomes:

$$V_{av} = V_D + SPV_{\max} D + SPV_{\max} f\tau_d \left(1 - e^{\frac{-(1-D)}{f\tau_d}} \right) \quad \text{(S5)}$$

This equation is consistent with the results of former "illumination modulated KPFM" reports.[5,6] Here, equation (5) is used to map the minority carrier lifetime in the polycrystalline silicon sample.

5 Taking into account two contributions to the surface photo-voltage

In the following, we assume that two mechanisms characterized by strongly different dynamics contribute to the surface photo-voltage. Their respective contributions to the average potential V_{av} can be taken into account by summing the integrals (Figure S4) of two components of the surface photo-voltage SPV_1 and SPV_2, each of them characterized by a set of independent parameters τb_i, τd_i, SPV^i_{max} (i=1,2) . Then, the average potential measured by KPFM (with respect to the in-dark potential V_D) is expressed as follow:

$$V_{av} = V_D + SPV^1{}_{\max} D\left(1 - e^{\frac{-D}{f\tau_{b1}}} e^{\frac{-(1-D)}{f\tau_{d1}}} \right) + SPV^1{}_{\max} \left(f\tau_{d1} - f\tau_{b1} \right) \left(1 - e^{\frac{-D}{f\tau_{b1}}} \right) \left(1 - e^{\frac{-(1-D)}{f\tau_{d1}}} \right) +$$
$$SPV^2{}_{\max} D\left(1 - e^{\frac{-D}{f\tau_{b2}}} e^{\frac{-(1-D)}{f\tau_{d2}}} \right) + SPV2_{\max} \left(f\tau_{d2} - f\tau_{b2} \right) \left(1 - e^{\frac{-D}{f\tau_{b2}}} \right) \left(1 - e^{\frac{-(1-D)}{f\tau_{d2}}} \right) \quad \text{(S6)}$$

With $\tau_{b1} >> \tau_{b2}$; $\tau_{d1} >> \tau_{d2}$

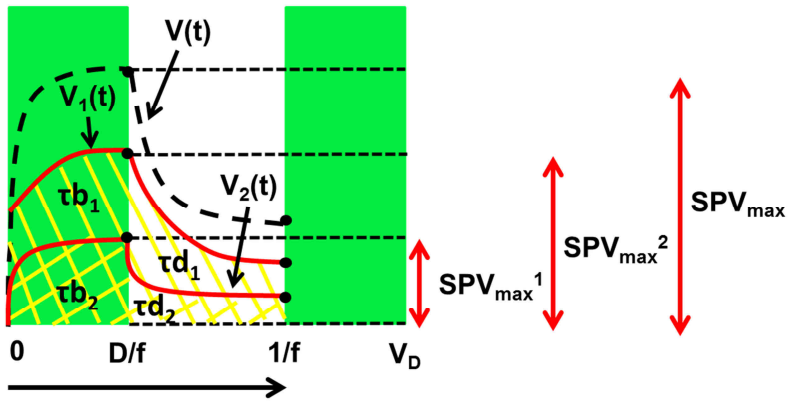

Figure S4. The surface potential V(t) is modeled by summing the contributions of two surface photo-voltage components, each of them being referenced with respect to the in-dark potential. In other words the surface photo-voltage V(t)-V_D is equal to $SPV^1(t)+SPV^2(t)$.

For the sake of simplicity, the first and second contributions will be referred as “slow” and “fast” SPV components, respectively. In order to clarify the frequency-behaviour of the average surface photo-voltage measured by KPFM, Figure S5 gives a schematic illustration of the surface potential time-response for increasing illumination modulation frequencies.

First, in the low frequency regime, photo-charging builds-up times (τb1, τb2) and photo-potentials decay times (τd1, τd2) are much smaller than the light pulses duration D/f and the time elapsed between two consecutive pulses $1-D/f$, respectively. Therefore, the temporal-averaged magnitude of each photo-potential contribution attains its maximum value during the light pulse and is equal to the in-dark surface potential V_D between the pulses. Under these conditions, the measured averaged photo-potential corresponds to the sum of the maximum magnitudes values of both components times the duty $\left(SPV^1{}_{\max}+SPV^2{}_{\max}\right)D$.

As the frequency increases, the time elapsed between consecutive pulses approaches and finally becomes shorter than the slowest decay time (τ_{d1}). Then, the slow SPV component does no more significantly decay between the light pulses, consequently increasing its average value over the modulation period. At this stage the faster average photo-potential contribution does not experience any significant change in its magnitude (because $\tau_{d2} << \tau_{d1}$). Further increase of the modulation frequency will prevent the appearance of the slowest SPV component as the light pulse duration becomes shorter than the slow photo-charging build-up time (τ_{b1}). Therefore, the global averaged photo-potential will decrease. Similar to the previous scenario, further increase of the modulation frequency will limit the decay of the faster photo-potential component between the light pulses, thus increasing again the averaged photo-potential. Further frequency-increase will shorten the light pulse duration below the faster photo-charging build-up time (τ_{b2}), preventing the faster SPV component development. At the very end the averaged photo-potential equals the in-dark surface potential.

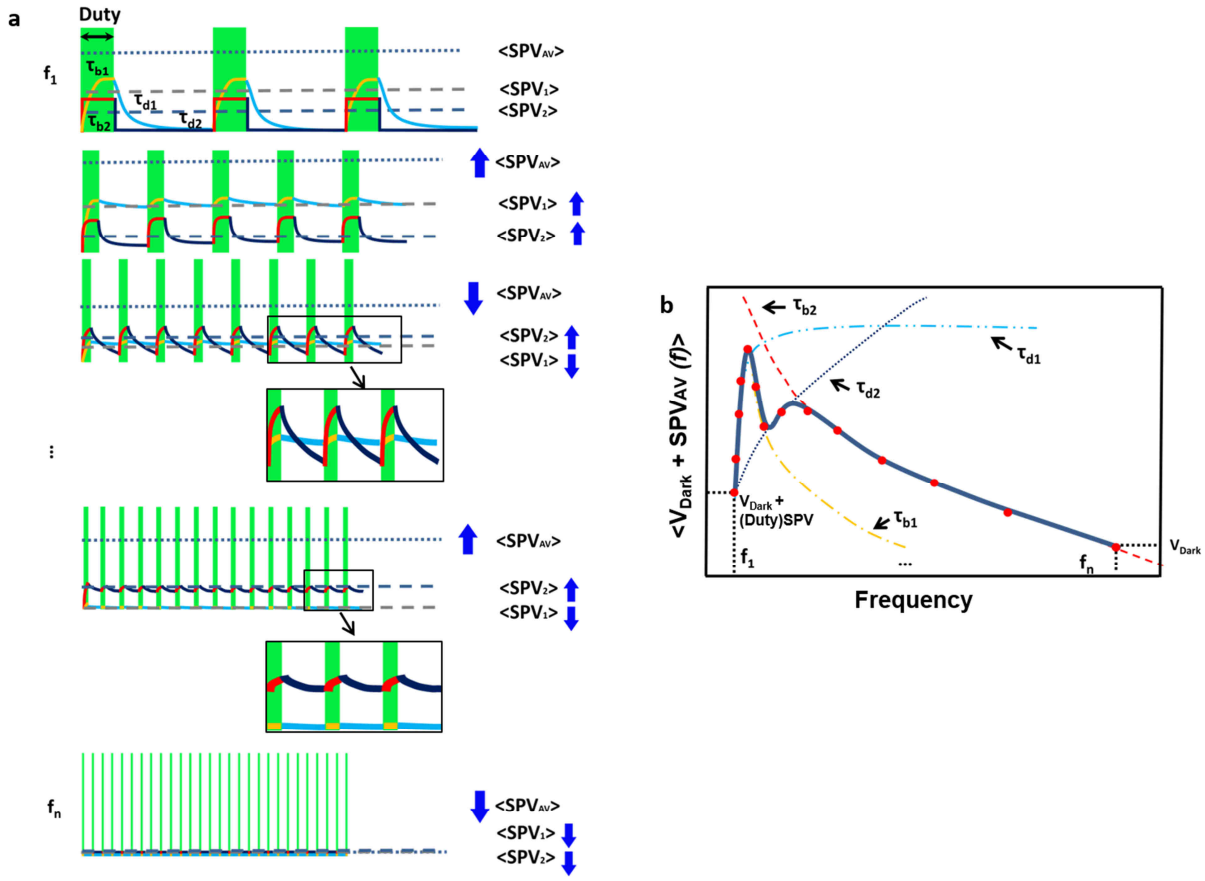

Figure S5. a) Surface potential time-response for increasing modulation frequencies. In this case the evolution of the average surface photo-voltage SPV_{av} is governed by two different built-ups (τb1 and τb2) and decays (τd1 and τd2) dynamics. b) Spectroscopy curve schematic. Guidelines for eye indicating the different dynamics contribution to the curve are given by dotted lines.

6 Fitting the average surface photo-potential with stretched exponentials

In some cases (see the discussion hereafter), it may be justified to use stretched exponentials to simulate the SPV dynamics. In principle, this could be done for both the SPV built-up and decay. In that case, equations 1, 2 and 4 would become:

$$0 \le t \le D/f \qquad SPV(t) = V(t) - V_D = K_1\left(1 - e^{\left(\frac{-t}{\tau_b}\right)^{\alpha}}\right) + K_2 \tag{S7}$$

$$D/f \le t \le 1/f \qquad SPV(t) = V(t) - V_D = K_3 e^{-\left(\frac{t-\frac{D}{f}}{\tau_d}\right)^{\beta}} \tag{S8}$$

$$V_{av} = V_D + SPV_{\max} D\left(1 - e^{\left(\frac{-D}{f\tau_b}\right)^{\alpha}} e^{-\left(\frac{-(1-D)}{f\tau_d}\right)^{\beta}}\right) + SPV_{\max}\left[\begin{array}{l} \frac{f\tau_d}{\beta}\Gamma\left(\frac{1}{\beta}, \left[\frac{1-D}{f\tau_d}\right]^{\beta}\right)\left(1 - e^{-\left(\frac{D}{f\tau_b}\right)^{\alpha}}\right) - \\ \frac{f\tau_b}{\alpha}\Gamma\left(\frac{1}{\alpha}, \left[\frac{D}{f\tau_b}\right]^{\alpha}\right)\left(1 - e^{-\left(\frac{(1-D)}{f\tau_d}\right)^{\beta}}\right) \end{array}\right] \tag{S9}$$

Here, $\Gamma(a,x)$ is the non-normalized lower-half Euler gamma function.

In the case of an instantaneous photo-charging (*i.e.* τb approaches zero), eq. 9 becomes:

$$V_{av} = V_D + SPV_{\max} D + SPV_{\max}\left[\frac{f\tau_d}{\beta}\Gamma\left(\frac{1}{\beta}, \left[\frac{1-D}{f\tau_d}\right]^{\beta}\right)\right] \tag{S10}$$

This last expression is consistent with the one derived by Shao and co-workers[7] for an instantaneous photo-generation (keeping in mind that D=0.5 in their case[7]).

7 Justification for non-using stretched exponentials

In the following, we motivate the non-utilization of stretched exponentials for fitting our data. Generally speaking, stretched exponential functions are used to describe dispersive kinetics where the characteristic time constant of the dynamical process changes with time.

In our case, the first SPV component accounts for the trap-filling and trap-delayed recombination processes. If one assumes in first approximation that both phenomena depend

only on a fixed trap density; their dynamics should be intensity-independent and one can use simple exponentials to describe both the “slow” SPV built-up (trap-filling) and decay (trap-delayed recombination) dynamics.

In turn, the non-geminate recombination of free carriers is an intensity-dependent second order process.[8] Therefore, in principle, one shall use a stretched exponential term to describe the decay of the “fast” SPV component. However, this approach is hardly applicable in our case. This is mostly due to the overlap of the different dynamical contributions to the SPV for frequencies up to 100 kHz, which prevents carrying out a reliable assessment of the stretched exponent that would yield an optimal fit of the “fast decay” component part of the curve, if taken alone. Moreover, as already mentioned, we stress that both the fast and slow built-up times increase when decreasing the optical power below a certain threshold. Then, in order to be totally rigorous, stretch exponentials (with independent stretch exponents) shall also be used to describe both SPV built-up dynamics. Performing such a fit is obviously unrealistic in our case. For these reasons, we made the choice to avoid unnecessary complications with the numerical fit procedure and used simple exponentials for all dynamical components.

Last, we want to briefly explain why it is not possible (at this stage) to overcome these issues by using an additional illumination source to work in a perturbative regime. Basically, this is what is done in a macroscopic transient photo-voltage (TPV) experiment.[9] During TPV measurements, the average carrier density is fixed by using a continuous white illumination source. A small optical perturbation is applied in such a way that the voltage transient is less than a few percent (typ. less than 5%, see Li and co-workers[10]) of the open circuit voltage average (which average value is determined by the carrier density).

In the case of KPFM experiments carried out on bare organic blends,[4,7,11-14] the surface photovoltage measured under continuous wave illumination is systematically reduced compared to the open circuit voltage of the full solar cell device with a top metallic electrode.[7] With photo-voltages of a few tens of mV, it becomes in practice impossible to operate KPFM under frequency-modulated illumination in a true non-perturbative regime. Indeed, the magnitude of the modulated photo-potentials would be only of a few mV, which is far insufficient to acquire spectroscopy-frequency curves with a proper signal to noise level.

8 Fitting procedure and calculation of surface photo-voltage and in-dark surface potential images

In this work, the dynamical image calculation is based on a point-by-point curve fit. In the case of measurements carried out on the poly-crystalline Si sample, a reduced set of variable parameters is used accordingly to equation 5: τd which represents the minority carrier lifetime, V_D which is the potential that would be measured without illumination and which is equal to the maximum photo-voltage measured under continuous wave illumination.

As explained previously, a dual set of variable parameters is in principle necessary to take into account the multiple dynamical contributions to the average surface potential measured on organic blends. The time-constant parameters are: τb1 (trap-filling), τd1 (trap delayed recombination), τb2 (free-carrier diffusion), τd2 (non-geminate recombination). Besides, a dual set of static photo-voltages components (SPV^1_{max} and SPV^2_{max}) is needed to account for the respective contributions of the “slow” and “fast” processes to the SPV magnitude. Again, V_D stands for the in-dark potential.

Concerning the dynamical time constants, only three parameters were used as variables during the fit. Indeed, as previously mentioned, the “fast” built-up time τb2 can only be estimated from simulations due to the frequency-limitations of the modulation chain. Its value was kept fixed below an upper limit (see the simulations hereafter) during the fit. The only exception is the one of the measurements carried out at the lowest intensities. In that case the increase of τb2 allows its direct determination from the spectroscopic curves.

To check the proper convergence of the fit, re-calculated images of the in-dark potential (i.e. images of fitted V_D values) were compared to real images of the potential recorded approximatively at the same location with the illumination source turned completely off. The calculated images (Figure S6) reproduce almost perfectly the experimental data, as shown by the comparison of cross-section profiles (Figure S6c). Besides, the dual set of static photo-voltage components (*i.e.* $SPV^1_{\max}$ and $SPV^2_{\max}$) can be summed to calculate an SPV image (Figure S6) equivalent to what would be measured under continuous wave illumination. Indeed, in the limit of an infinitely long light pulse, it can be easily shown that the surface photo-voltage is equal to $SPV^1_{\max} + SPV^2_{\max}$.

Last, a 2×2 Gaussian smooth filter was applied to the dynamical images to remove high frequency noise. As shown by Figure S7, the raw images display the same contrasts and features, but with a slightly higher noise level.

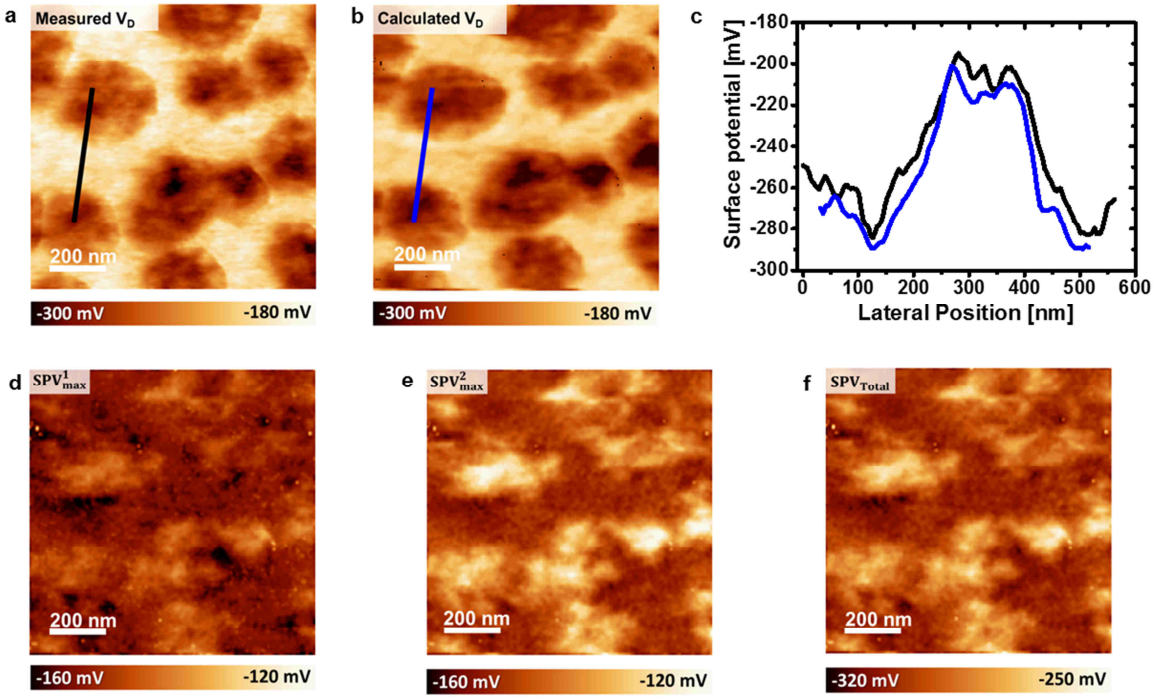

Figure S6. a) KPFM image (400x400 pixels, 1x1 μm) of the surface potential acquired in dark conditions on the large-scale heterogeneous $PC_{71}BM$:PDBS-TQx blend. This image has been recorded almost exactly at the same location than the dynamical images shown in Figure 2 (main text). b,d,e,f, series of calculated images (200x200 pixels, 1x1 μm) corresponding to the data shown in Figure 2 (main text). b) Calculated in-dark surface potential. c) Surface potential cross sections profiles corresponding to the path highlighted in black and blue in a and b, respectively. d,e) Images of the SPV^1_{max} (d) and SPV^2_{max} (e) parameters (see equation 6) calculated from the fit. f) Total surface photo-voltage image (*i.e.* $SPV^1_{max} + SPV^2_{max}$).

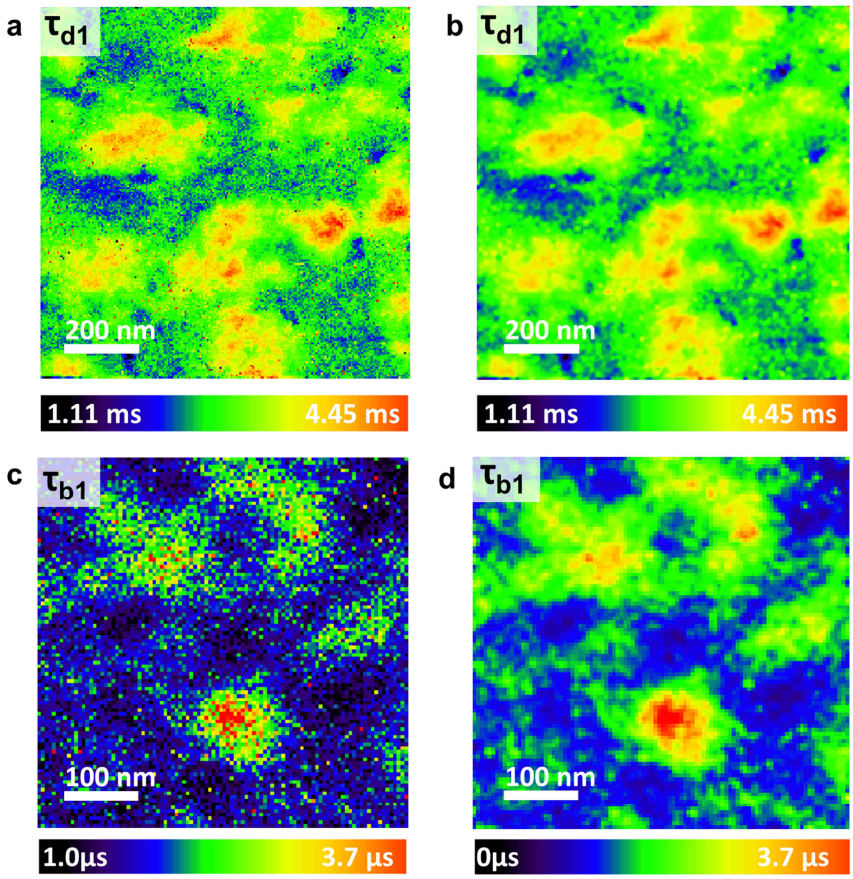

Figure S7. a,b) “slow” photo-voltage decay image of the large-scale heterogeneous PC71BM:PDBS-TQx blend (200x200 pixels, 1x1 µm) presented as raw data (a) and after applying a Gaussian smooth filter (b). c,d) “slow” photo-voltage built-up image of the nanophase segregated $PC_{71}BM$:PDBS-TQx blend (100x100 pixels, 500x500 nm) presented as raw data (c) and after applying a Gaussian smooth filter (d).

9 Estimating the “fast” built-up time from simulations

As above-mentioned, average photo-potential curves were simulated to estimate what would be the upper limit for the “fast” built-up ($\tau b2$) time constant. These simulations also demonstrated that fixing $\tau b2$ below its upper value does not influence the results (*i.e.* the values of the other variable parameters) of the curve fit. Last, for the lowest illumination intensities, the influence of the “fast” built-up becomes apparent on the spectroscopic curve. In that case the simulations were used to determine averaged $\tau b2$ values.

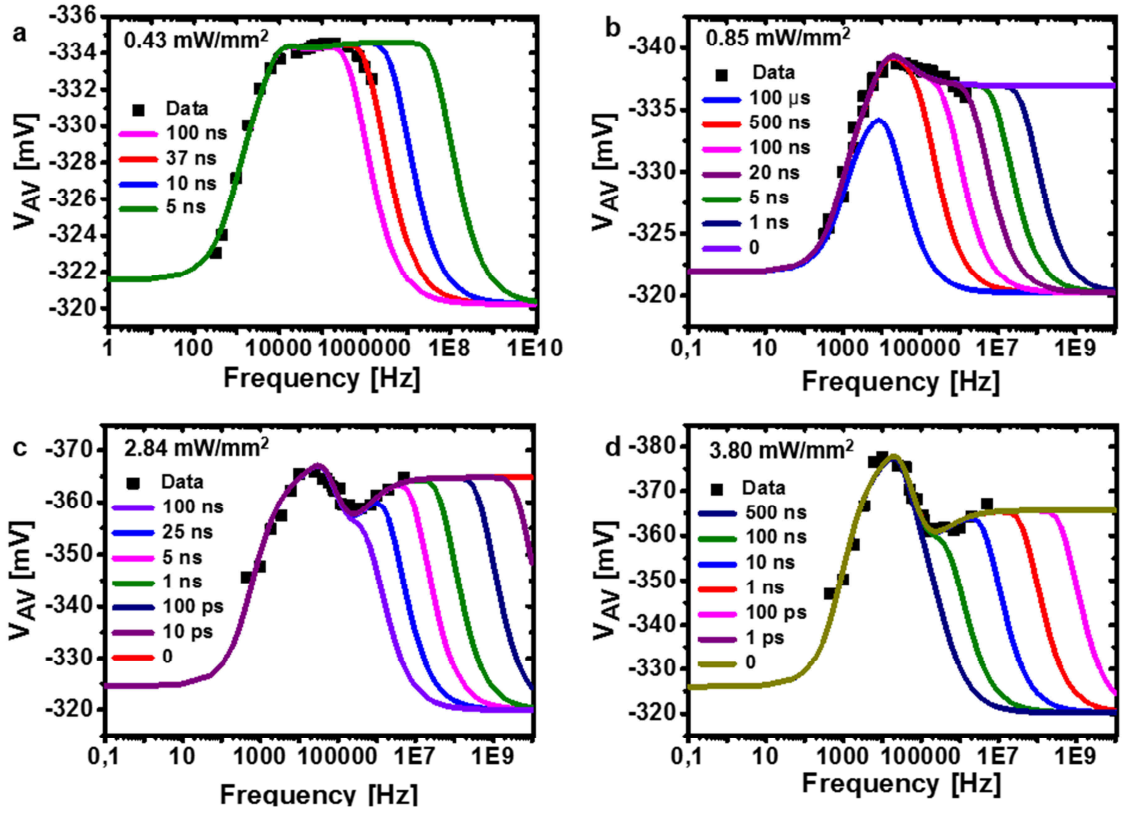

Figure S8. Spectroscopic curves of the average surface potential at different discrete frequencies (black squares) acquired for increasing optical powers on the nano-phase segregated $PC_{71}BM$:PDBS-TQx blend. The solid lines display the results of simulations for different τb2 values (all other parameters being kept constant accordingly to each illumination intensity). a,b) At low illumination intensities, the best adjustments are obtained for τb2= 37 ns and τb2= 20 ns at 0.43 mW/mm^2 and 0.85 mW/mm^2 , respectively. c,d) For these data, the "fast" built up time cannot be determined since its value is shorter than the time detection range allowed by the modulation chain. An upper limit can however be established by comparing the results of the simulations for different τb2 values.

10 Separating the contributions of four processes at the origin of the SPV contrast in the organic blends

Here, we illustrate the four processes which we assume to be at the origin of the slow and fast SPV built-up and decay dynamics observed in our experiments. The “fast” SPV built-up occurs after the exciton dissociation at the donor-acceptor interfaces. The “fast” built-up time constant $\tau b2$ represents the average time needed by the free charge carriers to diffuse in the D and A sub-networks. These carriers may eventually thermalize into trap states, which is a much slower process associated to the “slow” SPV built-up dynamics (time constant $\tau b1$). The free carriers can also non-geminately recombine at the donor-acceptor interfaces with a counter partner generated from another exciton dissociation event. This process is at the origin of the “fast” SPV decay dynamics (time constant $\tau d2$). Last, free charges can also recombine with a carrier released from a trap state with a time-constant $\tau d1$.

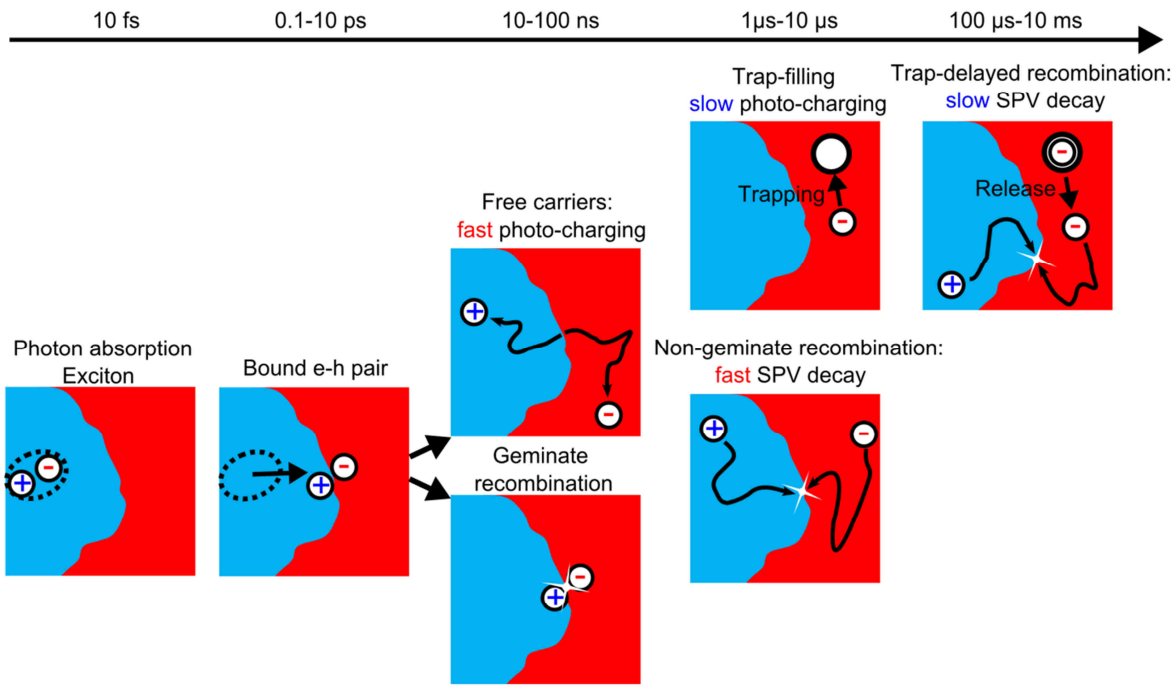

Figure S9. Schematic representations of events occurring at different timescales in a donor-acceptor blend. The electron-donor and electron-acceptor materials are represented in blue and red, respectively. The timescale is indicated in X-scale. The exciton generation diffusion to the D-A interface and separation into a charge transfer state (Coulomb-bound electron-hole pair) takes less than 1ns. Geminate recombination is usually supposed to occur on a time scale up to a few ns. Alternatively, the electron-hole pair can be fully separated into free charges. This process gives rise to a global sample photo-charging at the scale of a few tens of ns, identified in our measurements as the “fast” surface photo-voltage built-up process. The free carriers can thermalize into trap states at longer timescales. The trap-filling results in the development of a second photo-voltage component (*i.e.* slow photo-voltage). Last, the “fast” and “slow” surface photo-voltage decay dynamics are associated to the non-geminate and trap-delayed recombination processes, respectively. The later process is dominated by the slow dynamics of carrier-release from the trap states.

We stress that all of these processes contribute simultaneously to the “global” SPV measured by KPFM under continuous wave illumination. The powerfulness of multi-dynamical KPFM imaging resides in its ability to separate the contributions of these different processes, which is possible in our case because they occur at different timescales. For instance, at high modulations frequencies, the pulse width becomes too short to allow a proper thermalization of free carriers into trap states. As a consequence, at high frequencies the average SPV results only from the cumulative contributions of the free carrier diffusion and non-geminate recombination processes.

11 Minority carrier lifetime measurements in poly-crystalline Si

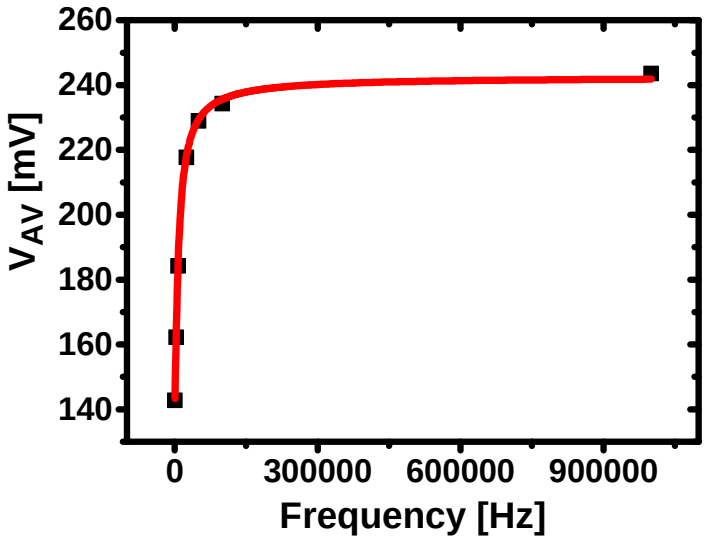

Figure S10. Single curve of the average surface potential as a function of the illumination modulation frequency acquired during the 2D dynamical imaging of the polycrystalline silicon sample. The numerical fit with equation 5 (red solid line) yields a single SPV decay time constant of 56.6 µs.

REFERENCES

1. Caffy, F.; Delbosc, N.; Chávez, P.; Lévêque, P; Faure-Vincent, J.; Travers, J.-P.; Djurado, D.; Pécaut, J.; Grévin, B.; Lemaitre, N.; Leclerc, N.; Demadrille, R. Synthesis, Optoelectronic Properties and Photovoltaic Performances of Wide Band-Gap Copolymers Based on Dibenzosilole and Quinoxaline Units, Rivals to P3HT. *Polym. Chem.* **2016**, 7, 4160-4175.

2. Cahen, D.; Kahn, A. Electron Energetics at Surfaces and Interfaces: Concepts and Experiments. *Adv. Mater*. **2003**, 15, 271-277.

3. Ellison, D. J.; Kim, J. Y.; Stevens, D. M.; Frisbie, C. Determination of Quasi-Fermi Levels across Illuminated Organic Donor/Acceptor Heterojunctions by Kelvin Probe Force Microscopy. *J. Am. Chem. Soc.* **2011**, 133, 13802-13805.

4. Fuchs, F.; Caffy, F.; Demadrille, R.; Mélin, T.; Grévin, B. High-Resolution Kelvin Probe Force Microscopy Imaging of Interface Dipoles and Photogenerated Charges in Organic Donor–Acceptor Photovoltaic Blends, *ACS Nano* **2016**, 10, 739-746.

5. Takihara, M.; Takahashi, T.; Ujihara, T. Minority Carrier Lifetime in Polycrystalline Silicon Solar Cells Studied by Photoassisted Kelvin Probe Force Microscopy. *Appl. Phys. Lett.* **2008**, 93, 021902.

6. Borowik, Ł.; Lepage, H.; Chevalier, N.; Mariolle, D.; Renault, O. Measuring the Lifetime of Silicon Nanocrystal Solar Cell Photo-Carriers by Using Kelvin Probe Force Microscopy and X-Ray Photoelectron Spectroscopy. *Nanotechnology* **2014**, 25, 265703.

7. Shao, G.; Glaz, M.; Fei, M.; Ju, H.; Ginger, D. Intensity-Modulated Scanning Kelvin Probe Microscopy for Probing Recombination in Organic Photovoltaics. *ACS Nano* **2014**, 8, 10799.

8. Cowan, S.; Roy, A.; Heeger, A. Recombination in Polymer-Fullerene Bulk Heterojunction Solar Cells. *Phys. Rev. B* **2010**, 82, 245207.

9. Shuttle, C.; O'Regan, B.; Ballatyne, A.; Nelson, J.; Bradley, D.; de Mello, J.; Durant, J. Experimental Determination of the Rate Law for Charge Carrier Decay in a Polythiophene: Fullerene Solar Cell. *Appl. Phys. Lett*. **2008**, 92, 093311.

10. Li, Z.; Gao, F.; Greenham, N; McNeill, C. Comparison of the Operation of Polymer/Fullerene, Polymer/Polymer, and Polymer/Nanocrystal Solar Cells: A Transient Photocurrent and Photovoltage Study *Adv. Energy Mater.* **2011**, 21, 1419-1431.

11. Hoppe, H.; Glatzel, T.; Niggemann, M.; Hinsch, A.; Lux-Steiner, M.; Sariciftci, N. Kelvin Probe Force Microscopy Study on Conjugated Polymer/Fullerene Bulk Heterojunction Organic Solar Cells. *Nano Lett.* **2005**, 5, 269-274.

12. Chiesa, M.; Bürgi, L.; Kim, J.-S.; Shikler, R.; Friend, R.; Sirringhaus, H. Correlation Between Surface Photovoltage and Blend Morphology in Polyfluorene-Based Photodiodes. *Nano Lett.* **2005**, 5, 559-563.

13. Maturova, K.; Kemerink, K.; Wienk, M.; Charrier, D.; Janssen, R. Scanning Kelvin Probe Microscopy on Bulk Heterojunction Polymer Blends. *Adv. Funct. Mater.* **2009**, 19, 1379-1386.

14. Spadafora, E.; Demadrille, R.; Ratier, B.; Grévin, B. Imaging the Carrier Photogeneration in Nanoscale Phase Segregated Organic Heterojunctions by Kelvin Probe Force Microscopy, *Nano Lett.* **2010**, 10, 3337-3342.